Journal of Applied Polymer Science

Effect of $BaTiO_3$ on the Microwave Absorbing Properties of Co-Doped Ni-Zn Ferrite Nanocomposites

Avinandan Mandal, Chapal Kumar Das
Materials Science Centre, Indian Institute of Technology, Kharagpur 721302, West Bengal, India
Correspondence to: C. Kumar Das (E-mail: chapal12@yahoo.co.in)

ABSTRACT: Coprecipitation and hydrothermal method were utilized for the synthesis of Co-doped Ni-Zn ferrite and barium titanate nanoparticles. The microwave absorption properties of Co-doped Ni-Zn ferrite/barium titanate nanocomposites with single layer structure were studied in the frequency range of 8.2–12.4 GHz.The spectroscopic characterizations of the nanocomposites were examined using X- ray diffraction, scanning electron microscopy, transmission electron microscopy and dynamic light scattering measurement. Thermogravimetric analysis indicated the high thermal stabilities of the composites. The composite materials showed brilliant microwave absorbing properties in a wide range of frequency in the X-band region with the minimum return loss of −42.53 dB at 11.81 GHz when sample thickness was 2 mm and the mechanisms of microwave absorption are happening mainly due to the dielectric loss. Compared with pure Co-doped Ni-Zn ferrite, Co-doped Ni-Zn ferrite/$BaTiO_3$ composites exhibited enhanced absorbing properties. The microwave absorbing properties can be modulated by controlling the $BaTiO_3$ content of the absorbers and also by changing the sample thicknesses. Therefore, these composites can be used as lightweight and highly effective microwave absorbers.
 J. Appl. Polym. Sci. **2014**, *131*, 39926.

KEYWORDS: composites; dielectric properties; thermogravimetric analysis (TGA)

Received 3 February 2013; accepted 1 September 2013
DOI: 10.1002/app.39926

INTRODUCTION

In recent years, electromagnetic waves in the gigahertz frequency range are enormously used in wireless communication tools, local area networks, radar systems, etc. The increasing usage of electromagnetic wave devices results in electromagnetic interference problem in both civil and military applications. To overcome this problem, a class of materials are used which have strong electromagnetic wave absorbing properties. The absorbers attenuate the electromagnetic energy through its dielectric or magnetic loss. In the present article, we have motivated on the development of electromagnetic wave absorbing materials mainly for military purposes.[1–3] Reduction of radar signature of military platforms is a challenging issue during the Second World War. The main goal is that the development of excellent radar absorbing materials (RAMs) with light weight, smaller thicknesses that absorb strong microwave radiation over a wide frequency range. These types of materials are used to minimize the electromagnetic reflection from metal surfaces such as aircrafts, ships, tanks, etc. From the literature survey, it is seen that different types of magnetic and dielectric materials are used to develop radar absorbing materials.[4–10] Magnetic material such as spinel type compound are widely applied as absorbing materials because of their high specific resistance, remarkable flexibility in tailoring the magnetic properties and ease of preparation.[11,12] Recently, it has been shown that magnetic nanocomposites are used as absorbing materials due to their advantages in respect to light weight, low cost and better microwave properties over pure ferrites.[13,14] Several groups have reported good microwave absorption properties of $Ni_{0.5}Zn_{0.5}Fe_2O_4$/bamboo charcoal,[15] Ag-coated Ni-Zn ferrite core-shell nanopowders,[16] Nd-doped Ni-Zn ferrites,[17] carbonyl iron/Ni-Zn ferrite composites,[18] SiC coated Fe_2O_3 and Fe_3O_4,[19] Fe_3O_4/$BaTiO_3$ composites,[20] etc. Our group investigated the microwave absorbing properties of DBSA-doped polyaniline/$BaTiO_3$-$Ni_{0.5}Zn_{0.5}Fe_2O_4$ nanocomposites that showed also good microwave absorbing properties.[21] In order to enhance the absorbing properties, the polarizability of nickel zinc ferrite was amplified by cobalt doping.[22] Spinel type soft ferrites are the most popular and effective microwave absorbers in the megahertz range, but its absorbing property reduces due to Snoek's limit when frequency ups to gigahertz.[23] Magnetic-dielectric composite absorption materials were fabricated by ball milling in order to achieve the excellent absorbing properties. Barium titanate is a dielectric material having permanent polarizations which can be used as microwave absorber. In this article, $Co_{0.2}Ni_{0.4}Zn_{0.4}Fe_2O_4$/$BaTiO_3$ composite absorption materials

were fabricated by ball milling and these types of composite materials can have high dielectric and magnetic loss due to interaction between electric polarization and magnetization.[5] Complex relative permittivity ($\varepsilon_r = \varepsilon' - j\varepsilon''$) and permeability ($\mu_r = \mu' - j\mu''$) of the developed composites were measured by employing vector network analyzer (model ENA E5071C) and with the help of these values, input impedance (Z_{in}) was calculated by using an equation: $z_{in} = z_0\sqrt{(\mu_r/\varepsilon_r)}\tanh\left[(-j2\pi/c)\left(\sqrt{\varepsilon_r\mu_r}\right)fd\right]$. The microwave absorbing properties of the RAMs were represented by the return loss (R_L) which is calculated by using an equation: $R_L = -20\log_{10}\left[\left|\frac{(z_{in}-z_0)}{(z_{in}+z_0)}\right|\right]$,[24] where z_{in} is the characteristic input impedance and z_0 is the free space impedance. c is the velocity of light, f is the frequency of microwaves and d is the thickness of absorber. Better result comes when the characteristic input impedance is close to the free space impedance (377 Ohms). The input impedance depends on permittivity, permeability, thickness of an absorber and also on the operating frequency. So the surface reflectance of an absorber is a function of six characteristic parameters, namely ε', ε'', μ', μ'', f and d. The developed RAMs showed superior absorbing properties in a wide frequency range in the X-band region with a minimum return loss of −42.53 dB at 11.81 GHz when sample thickness was 2 mm. The absorption mechanisms have been explained with the help of real and imaginary parts of complex relative permittivity and permeability.

EXPERIMENTAL

Materials

Nickel nitrate ($Ni(NO_3)_2.6H_2O$), zinc nitrate ($Zn(NO_3)_2.6H_2O$), cobalt nitrate ($Co(NO_3)_2.6H_2O$) and ferric nitrate ($Fe(NO_3)_3.9H_2O$) of analytical reagent grade were purchased from Merck Chemicals (India). Barium nitrate ($Ba(NO_3)_2$), titanium tetrachloride ($TiCl_4$), sodium hydroxide (NaOH) and potassium hydroxide (KOH) were obtained from Lobachemie (India). All reagents were used without further purification and distilled water was used in all the experiments.

Preparation of $Co_{0.2}Ni_{0.4}Zn_{0.4}Fe_2O_4$ Nanoparticles

Nanocrystalline $Co_{0.2}Ni_{0.4}Zn_{0.4}Fe_2O_4$ particles were prepared by coprecipitation method.[22] Aqueous solution of $Fe(NO_3)_3.9H_2O$, $Co(NO_3)_2.6H_2O$, $Zn(NO_3)_2.6H_2O$ and $Ni(NO_3)_2.6H_2O$ in the respective stoichiometry were mixed thoroughly using a magnetic stirrer at 80°C. Then this solution was immediately transferred into a boiling solution of NaOH (molar ratio of OH/Co-doped Ni-Zn ferrite was taken 8) and stirred continuously for 60 min at 100°C. The resulting suspension was washed several times with water and twice with acetone. The powders were recovered by filtration, dried at 60°C and calcined 2 h at 600°C to promote formation of spinel phase.

Preparation of $BaTiO_3$ Particles

$BaTiO_3$ particles were prepared by hydrothermal processes.[25] $TiCl_4$ was dissolved in the ethanol first and then $Ba(NO_3)_2$ was added in the $TiCl_4$-ethanol solution with continuous stirring. KOH solution was added drop wise into the mixed solution until it changes into gelatin. The gel was aged in air for 8 h and the gel was hydrothermally treated in autoclave at 240°C for 8 h. At last, the powders were calcined at 1100°C to develop $BaTiO_3$ phase (perovskite).

Table I. Compositions and Minimum Return Loss Values of the Nanocomposites with Different Thicknesses

Sample code	Composition (30% filler)	Thickness (mm)	Minimum return loss (−dB)	Frequency (GHz)
RAM-1	Co-doped NZF	2	25.99	12.4
		2.5	**27.15**	**10.21**
		3	26.22	8.95
RAM-2	Co-doped NZF/ $BaTiO_3$(3:1)	2	28.65	12.15
		2.5	28.31	10.8
		3	**29.13**	**9.54**
RAM-3	Co-doped NZF/ $BaTiO_3$ (1:1)	**2**	**42.53**	**11.81**
		2.5	38.55	10.55
		3	39.83	9.29
RAM-4	Co-doped NZF/ $BaTiO_3$ (1:3)	2	33.19	11.73
		2.5	**36.22**	**10.54**
		3	34.60	9.54
RAM-5	$BaTiO_3$	2	27.96	11.39
		2.5	27.38	10.22
		3	**29.66**	**9.27**

Preparation of Microwave Test Plate

The compositions and minimum return loss values of the prepared RAMs were illustrated in Table I. Co-doped Ni-Zn ferrite nanoparticles were individually dispersed in epoxy resin matrix to develop RAM-1. Co-doped NZF and $BaTiO_3$ particles were mixed separately in three different ratios, 3:1, 1:1, 1:3 by using a horizontal type common ball mill. Ball to powder weight ratio was taken 10:1 and speed of the ball mill was ~225 RPM. We used epoxy resin (LY556) as a polymeric matrix because of its better adhesive property, superior mechanical properties, etc. Epoxy resin (bisphenol A diglycidyl ether) is formed by reacting two moles of epichlorohydrin with one mole of bisphenol A. The linear epoxy resin reacts with ethylene di-amine to form a three dimensional cross linked thermoset structure. The prepared mixed powders were dispersed in epoxy resin matrices at 80°C with the help of mechanical stirrer for 1 h and cured at 75°C for 30 min and designated as RAM-2, RAM-3, and RAM-4 respectively. Only $BaTiO_3$ particles were dispersed in polymeric matrix as RAM-5. Filler concentration was kept as ~30% in all the samples and thickness of all the samples were taken between 2 mm to 3 mm. All the samples were cut into desired rectangular shape of (0.4 in x 0.9 in) to fit into the X - band waveguide for microwave measurement.

CHARACTERIZATION

The phase analyses of the nanomaterials were done by employing X-ray diffraction (XRD), Rigaku X-ray

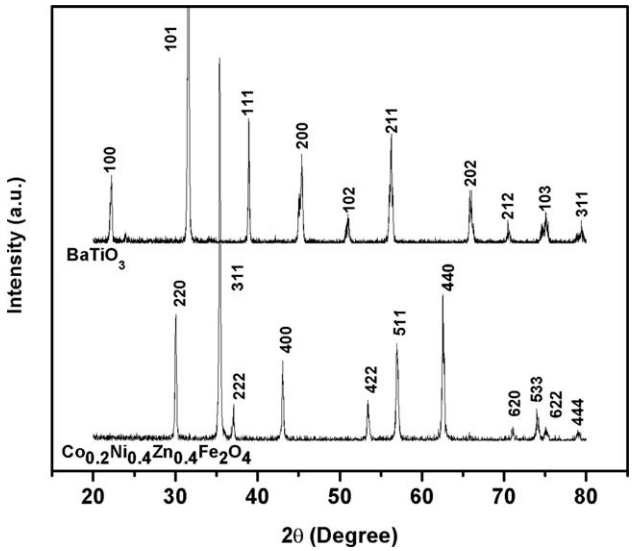

Figure 1. XRD pattern of Co-doped Ni-Zn ferrite ($Co_{0.2}Ni_{0.4}Zn_{0.4}Fe_2O_4$) and $BaTiO_3$ nanoparticles.

Diffracrometer, ULTIMA III with Cu Kα radiation ($\lambda = 1.5418$ Å). Scanning electron microscopy (SEM), VEGA, TESCAN was utilized to examine about the surface morphology of the composites. To get the size distribution of the particles, we utilized a Malvern Nano ZS instrument employing a 4 mW He−Ne laser ($\lambda = 632.8$ nm) for dynamic light scattering measurements. All of the scattering photons were collected at a 173° scattering angle. The scattering intensity data were processed using the instrumental software to obtain the hydrodynamic diameter (d_h). To know the shape of fillers of the composites, we have employed transmission electron microscopy (TEM), JEOL JEM-2100 microscope. Energy-dispersive X-ray spectroscopy (EDS) attached to TEM, while EDX analysis was performed to understand their chemical constituents. Thermo gravimetric analysis (TGA) was obtained on DuPont TGA-2100 thermal analyzer in the temperature range 30–700°C with a heating rate of 10°C/min. The magnetic properties were measured using a Quantum Design Evercool SQUID-VSM magnetometer with an applied magnetic field strength over the range from −10 kOe to +10 kOe at room temperature. The real and imaginary parts of complex relative permittivity and permeability were measured employing Agilent vector network analyzer (ENA E5071C).

RESULTS AND DISCUSSION

Structure Characterization

Figure 1 is the spectrum of XRD for $Co_{0.2}Ni_{0.4}Zn_{0.4}Fe_2O_4$ and $BaTiO_3$ particles. The main peaks of $Co_{0.2}Ni_{0.4}Zn_{0.4}Fe_2O_4$ are located at $2\theta =$ 30.08°, 35.43°, 37.07°, 43.06°, 53.43°, 56.95°, 62.54° and 73.99°. The peaks of $Co_{0.2}Ni_{0.4}Zn_{0.4}Fe_2O_4$ are accordant to that of reference data (JCPDS, PDF no. 04-002-0423),which gestured as face centered cubic spinel structure. No impurity peaks were seen in the spectrum, which indicated that high purity crystalline $Co_{0.2}Ni_{0.4}Zn_{0.4}Fe_2O_4$ was synthesized. The main peaks of barium titanate situated at $2\theta =$ 22.23°, 31.51°, 38.90°, 45.36°, 51.08°, 56.28°, 65.78°, 70.38°, 75.07° and 79.43° are match with the reference data (JCPDS, PDF no. 04–009-3215), which can be identified as tetragonal perovskite structure without any impurity.

Figure 2(a) is the SEM image of RAM-3 in the secondary electron detector (SE detector). It was shown that the nanoparticles were uniformly dispersed into the polymeric matrix with small agglomeration. Figure 2(b) is the SEM image of RAM-3 in the backscattered electron detector (BSE detector). The bright spot in Figure 2(b) indicated the heavy particles that were spread into the polymeric matrix.

Size distributions by number of the particles are shown in Figure 3. Co-doped NZF and barium titanate particles were dispersed separately in distilled water by sonication for 1 h and

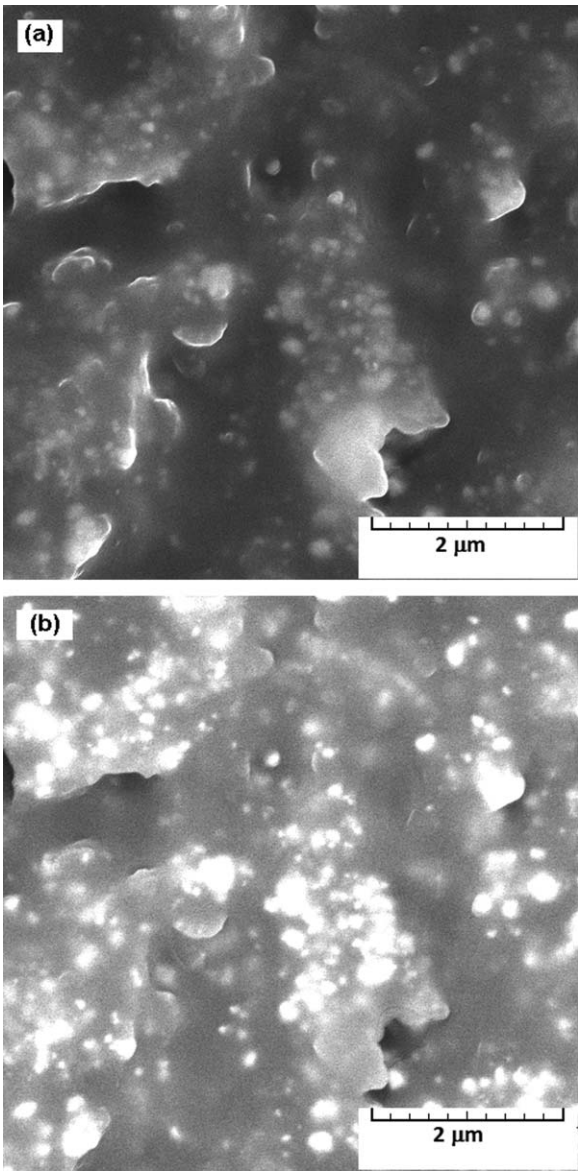

Figure 2. (a) SEM image of RAM-3 in the secondary electron detector (SE). (b) SEM image of RAM-3 in the backscattered electron detector (BSE).

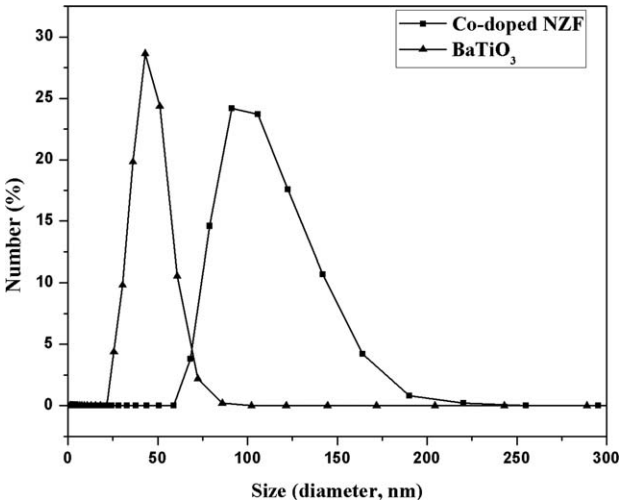

Figure 3. Size distribution of the Co-doped NZF and $BaTiO_3$ nanoparticles.

these two solutions were used to perform the dynamic light scattering test. We studied the size distribution of the particles with respect to the number of the particles. In a typical size distribution graph from the DLS measurement, the x-axis shows a distribution of size classes in nanometers, while the *y*-axis shows the number percentage of the particles. The average particle size of Co-doped NZF and BaTiO3 particles are 107 nm and 51 nm, respectively.

Figure 4(a) is the TEM image of the Co-doped NZF nanoparticles. In the coprecipitation method, cubic shaped Co-doped NZF nanoparticles were formed with different particle size. TEM images of $BaTiO_3$ nanoparticles indicated that the nanoparticles were almost spherical in shape [Figure 4(b)]. Cubic and spherical shaped magnetic and dielectric nanoparticles were dispersed in the polymeric matrix as shown in Figure 4(c). Figure 4(d) is the EDS spectrum which was analyzed in a small area [within the square bracket in Figure 4(c)]. EDS spectrum revealed the presence of oxygen (O), carbon (C), barium (Ba), titanium (Ti), cobalt (Co), nickel (Ni), zinc (Zn), and iron (Fe) and no contaminated element was detected. EDS spectrum showed the presence of high amount of Cu as the TEM samples were prepared on Cu-grids.

Thermal Stability

Thermal stability of the developed composite materials was investigated by thermo-gravimetric as shown in Figure 5. Fillers were uniformly dispersed in epoxy resin polymeric matrix and due to heat shielding effect of fillers, the segmental motions of epoxy resin have been obstructed. For this reason, RAMs showed higher thermal stability than pure epoxy (without adding any filler). Significant TGA data of the composite materials were recorded in Table II. The degradation temperature at 10% weight loss for RAM-3 was higher than the other composites. RAM-3 acquired maximum polarizations as RAM-3 contained an equal concentration of dielectric and magnetic materials in the polymer matrix. The dominant polarizations increased the thermal stability of the composite. The degradation temperature at 80% weight loss for pure epoxy was 425°C but at this temperature, the composites were thermally stable. Hence the thermal stability of epoxy has enormously increased by the addition of fillers.

Dielectric and Magnetic Properties

The mixed powders were pressed to form rectangular shapes with a particular dimension and the real part of complex relative permittivity i.e. dielectric constant values of these mixed powders have measured in the X-band region. The variation of dielectric constant values of the powders with frequency at room temperature are shown in Figure 6. $BaTiO_3$ showed the dielectric constant of 119 and the composite materials showed the values less than that of $BaTiO_3$ powders. $BaTiO_3$ have permanent electric dipoles and orientation polarizations of these dipoles are responsible for the high dielectric constant. For this reason, the dielectric constant values were decreased with decreasing barium titanate concentration in the composites. The values of dielectric constant of the powders were also decreased with increasing frequency i.e. the dielectric properties of the powders were dependent on frequency. At higher frequency, the external electric field changes rapidly and the realignment of the electric dipoles with the external field is very difficult due to the viscosity of the materials. As a consequence polarizations created by the electric dipoles are diminished with increasing frequency.

The magnetic properties of the as-synthesized Co-doped NZF and the representative Co-doped NZF/$BaTiO_3$ nanocomposites were measured using a vibrating sample magnetometer (VSM) at room temperature with an external field $-10\ \text{kOe} \leq H \leq 10$ kOe, as shown in Figure 7. In case of Co-doped NZF, saturation magnetization (M_s), remnant magnetization (M_r), and coercive force (H_c) were estimated to be $M_s = 22$ emu/g, $M_r = 6.8$ emu/g, $H_c = 101.7$ Oe repectively. The result indicated the paramagnetic behavior of the Co-doped NZF nanoparticles. A similar behavior for the Co-doped/$BaTiO_3$ nanocomposites was observed. In contrast, M_s of the Co-doped NZF/$BaTiO_3$ nanocomposites were decreased gradually with increasing volume of nonmagnetic particles to the total sample volume.

Microwave Absorbing Properties

The microwave absorbing properties of RAMs in the X-band region are shown in Figure 8(a–e). RAM-1 showed a broad peak with the minimum return loss of −27.15 dB at 10.21 GHz when thickness was 2.5 mm [Figure 8(a)]. From Figure 8(b) it was clearly seen that RAM-2 exhibited a minimum return loss of −29.3 dB at 9.54 GHz when thickness was 3 mm. RAM-3 was optimal radar absorbing material by showing minimum return loss of −42.53 dB at 11.81 GHz with 2 mm absorber thickness [Figure 8(c)]. From Figure 8(d,e), RAM-4 and 5 exhibited a minimum return loss of −36.22 at 10.54 GHz and −29.66 dB at 9.27 GHz when thickness was 2.5 mm and 3 mm, respectively. RAM-1 contained only Co-doped nickel zinc ferrite and from RAM-2 to 4, the concentration of barium titanate increases. RAM-5 contained only barium titanate. Better performance is substantiated when

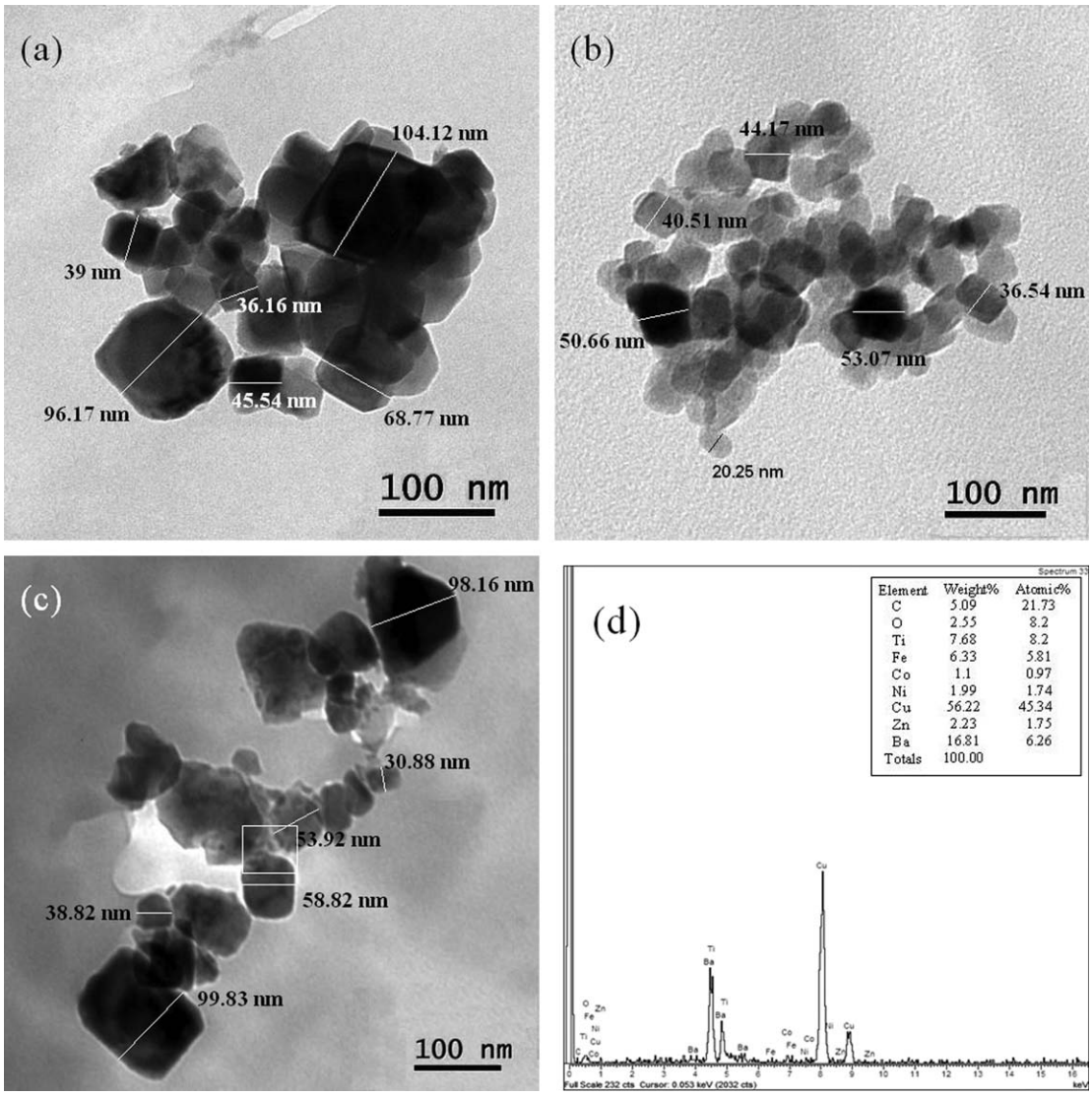

Figure 4. (a) TEM image of Co-doped Ni-Zn ferrite nanoparticles. (b) TEM image of $BaTiO_3$ nanoparticles. (c) TEM image of RAM-3. (d) EDS study of RAM-3.

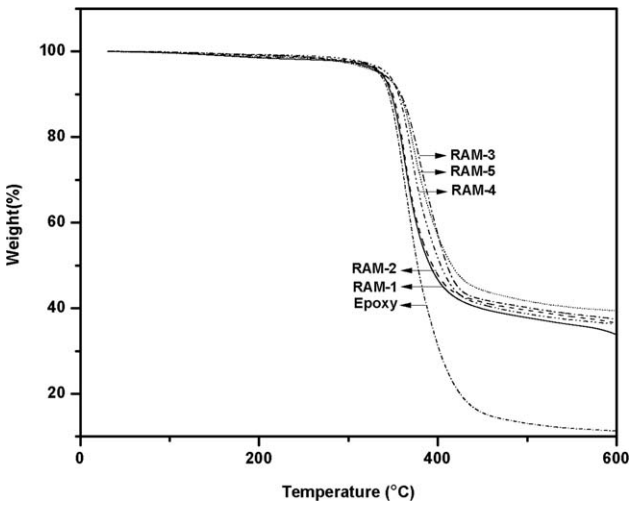

Figure 5. TGA of the composite materials.

both the magnetic and dielectric media are present within the system. Table III shows a comparative study of absorbing properties of the present RAMs with other related works.[15–21,26–30]

Table II. Data of TGA Analysis for the Composites

Sample	Degradation temperature	
	at 10% weight loss (T_{10}°C)	at 80% weight loss (T_{80}°C)
Pure epoxy	346	425
RAM-1	348	-
RAM-2	350	-
RAM-3	359	-
RAM-4	356	-
RAM-5	357	-

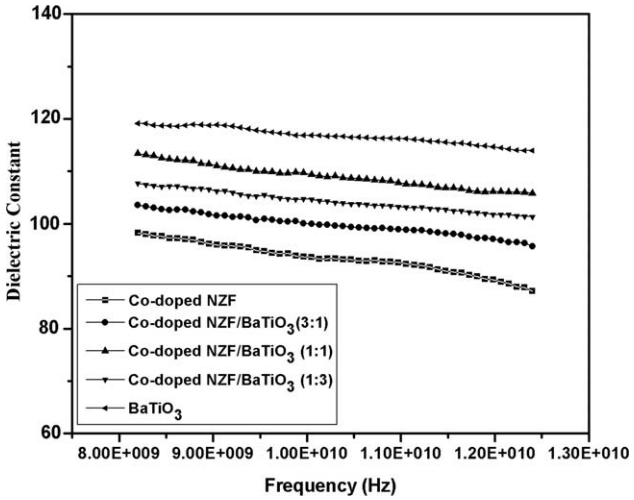

Figure 6. Dielectric properties of the mixed powder before embedded in the epoxy matrix.

Permittivity and Permeability Spectra

The real and imaginary parts of complex permittivity and permeability values were measured for all the absorbers due to investigate the appropriate mechanism of microwave power absorption. The real parts of complex permittivity (ε'), permeability (μ') stand for energy storage part and the imaginary parts of permittivity (ε'') and permeability (μ'') stand for energy loss part. The real and imaginary permittivity and permeability are shown in Figure 9(a–d). The values of real parts of permittivity (ε') value i.e. electric energy storage parts for RAM-1, 2, 3, 4 and 5 were approximately 3.5, 3.65, 3.95, 3.76, and 4.5, respectively [Figure 9(a)]. The dielectric constant (ε') values of the absorbers have been increased with increasing BaTiO3 concentration except RAM-3. Dielectric constant depends on two factors, orientation and interfacial polarizations. BaTiO3 has face centered cubic structure in which Ti^{4+} ions form 6-fold coordination, surrounded by octahedron of O^{2-} ions and Ba^{2+} ions situate at the corners i.e., form 12-fold coordination. At room temperature, possibly due to the low energy position of Ti^{4+} ions, the Ti^{4+} ions are off-centered. As a result, octahedrons are distorted and due to this distortion, BaTiO3 has permanent electric dipoles and show orientation polarization.[31] RAM-5 (30% BaTiO3) acquired higher dielectric constant value than other RAMs as its orientation polarization should be high. But exceptionally RAM-3 exhibited better dielectric constant value than RAM-4. This might be attributed due to better interfacial polarization than other absorbers as RAM-3 contained the equal percentage of ferromagnetic and ferroelectric materials. The imaginary parts of permittivity (ε'') i.e. electric energy loss parts for RAM-1, 2 were ~0.11 and for RAM-3, it was ~0.22. The ε'' values for RAM-4 and 5 were approximately 0.16 [Figure 9(b)]. The electric energy loss is responsible for the dielectric relaxation phenomena. The dielectric relaxation phenomena should be high for RAM-3 as it showed the higher ε'' value than other RAMs. The ε'' values for all RAMs were dependent on frequency with some peak points that were caused due to relaxation phenomenon resulting dissipation of microwave energy as heat. RAM-5 contains only $BaTiO_3$ but it's dielectric loss value i.e. ε'' fluctuates with frequency. The ε'' value is increased tremendously from frequency 8.2 GHz to 8.6 GHz because at this frequency range, the dielectric relaxation phenomena may be high.

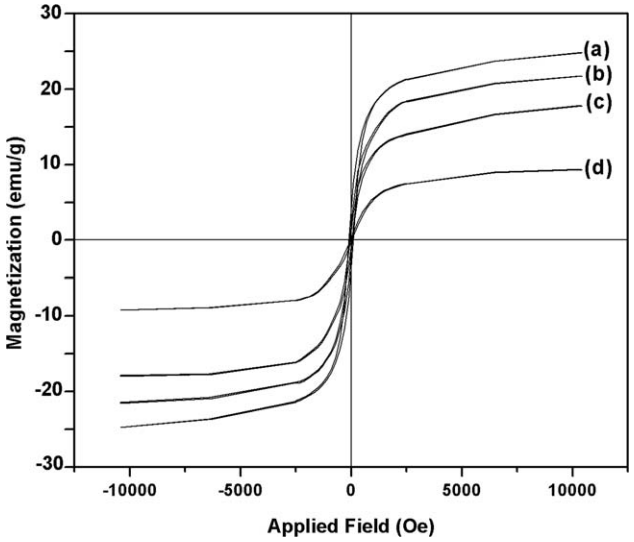

Figure 7. Magnetization curves of (a) pure Co-doped NZF, (b) Co-doped NZF/BaTiO3 (3:1), (c) Co-doped NZF/BaTiO3 (1:1), and (d) Co-doped NZF/BaTiO3 (1:3) composites.

The values of real parts of permeability (μ') i.e. magnetic energy storage parts for all the materials lie from 1.15 to 1 and μ' values were decreased with increasing frequency [Figure 9(c)]. The value of imaginary parts of permeability (μ'') i.e. magnetic energy loss parts for RAM-1 lie from 0.13 to 0.04 and the μ'' values were reduced from RAM-1 to RAM-5 [Figure 9(d)]. The μ'' values of the RAMs were dependant on the concentration of the magnetic ferrite particles and magnetic energy loss occurred due to eddy-current loss and residual loss.[32] In this study, the enhancement of eddy loss might be contributed to higher μ'' of the Co-doped NZF/$BaTiO_3$ composites because of $BaTiO_3$ being a ferroelectric material with band gap 3.2 eV.[5,33] Especially, when the weight ratio of Co-doped NZF/$BaTiO_3$ was 1:3, the μ' and μ'' of the Co-doped NZF/$BaTiO_3$ composite showed the maximum value. At higher frequency in the gigahertz range, as the external field changes rapidly, the realignment of magnetic dipoles with the external field is too difficult, for this reason the real part of permeability (μ') decreases with increasing frequency and so also μ'' values decreases with increasing frequency.

Since the present system was a heterogeneous system, the interfacial polarization process might have occurred at the interfaces between nanofillers and polymer matrices.[34] The permanent polarizations, dominant polarizations and their associated relaxation phenomena constitute the loss mechanism. Composite materials that contained both dielectric and magnetic media in polymeric matrix, there occurred an additional dielectric interfaces and more polarization charges on the surface of the particles make the dielectric relaxation more

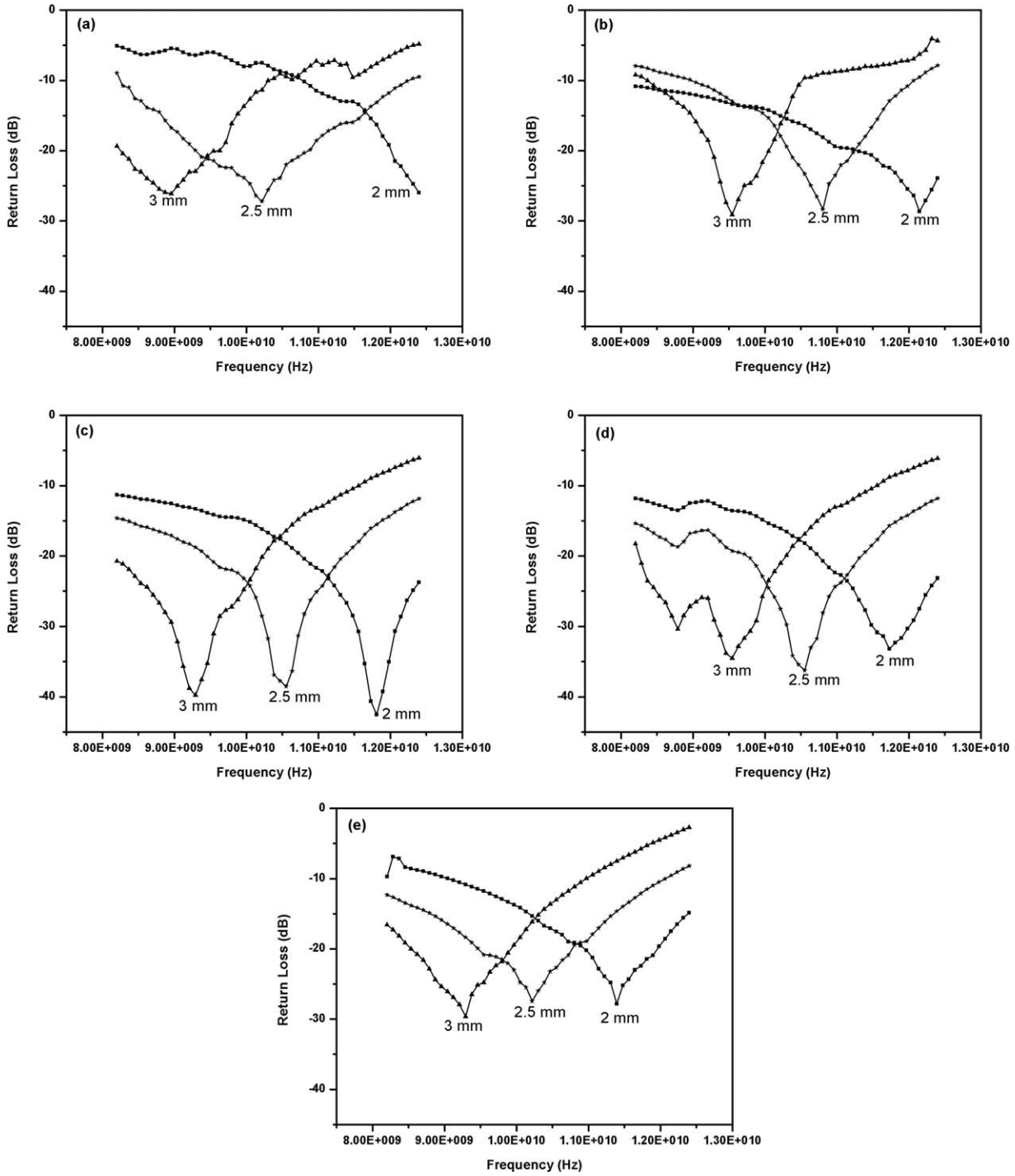

Figure 8. Microwave absorbing properties with different thicknesses of (a) RAM-1, (b) RAM-2, (c) RAM-3, (d) RAM-4, and (e) RAM-5.

complex.[35] From the above results, it was seen that the nanocomposites showed absorbing properties in order to dielectric loss tangent ($\varepsilon''/\varepsilon'$) i.e. dielectric loss was mainly responsible for the microwave power absorption. Other factors i.e. real and imaginary parts of permeability were also responsible for absorption. Return loss values of the present composites have been calculated from the expression: $R_L = -20\log_{10}\left[\left|\frac{(z_{in}-z_0)}{(z_{in}+z_0)}\right|\right]$. Better result comes when the characteristic input impedance (z_{in}) is close to the free space impedance ($z_0 = 377$ Ohms). The characteristic input impedance is expressed by the equation- $z_{in} = z_0\sqrt{(\mu_r/\varepsilon_r)}\tanh\left[(-j2\pi/c)\left(\sqrt{\varepsilon_r\mu_r}\right)fd\right]$. The input impedance is dependent on permittivity, permeability, operating

Table III. Comparison of Microwave Absorbing Properties of the RAMs with Other Studies

Sample	Minimum return loss (dB)	Frequency (GHz)	Thickness(mm)	Ref.
$Ni_{0.5}Zn_{0.5}Fe_2O_4$/bamboo charcoal	−13.4	7.4	2	15
Ag-coated Ni-Zn ferrite core-shell	−33.53	13.76	1.24	16
Nd-doped Ni-Zn ferrite	−20.7	12	2	17
carbonyl iron/Ni-Zn ferrite	−26.7	0.86	6	18
SiC coated Fe_2O_3 and Fe_3O_4	−15.6	9.6	2	19
$Fe_3O_4/BaTiO_3$	−22	8.3	2	20
DBSA-PANI/$BaTiO_3$-$Ni_{0.5}Zn_{0.5}Fe_2O_4$	−15.78	10.8	2	21
$SrFe_{11.2}Zn_{0.8}O_{19}$	−29.81	10.37	2.5	26
Ba-CoTi hexaferrite composites	−24	9.9	2.8	27
$SrFe_{12}O_{19}/CoFe_2O_4$ ferrite	−27.6	10.8	2	28
$BaFe_{12}O_{19}/TiO_2$ nanocomposites	−38.0	13.2	3	29
Ni/$SrFe_{12}O_{19}$ magnetic powder	−41.3	9.2	3	30
This work	−42.53	11.81	2	–

frequency and thicknessess of the absorbers The value of Z_{in} is close to the value of Z_0 when dielectric contribution matches the magnetic contribution i.e. the mathematical expression $\sqrt{(\mu_r/\varepsilon_r)}\tanh\left[(-j2\pi/c)\left(\sqrt{\varepsilon_r\mu_r}\right)fd\right]$ is close to 1 i.e. microwave absorption is directly dependent on dielectric and magnetic contribution of the absorbers.

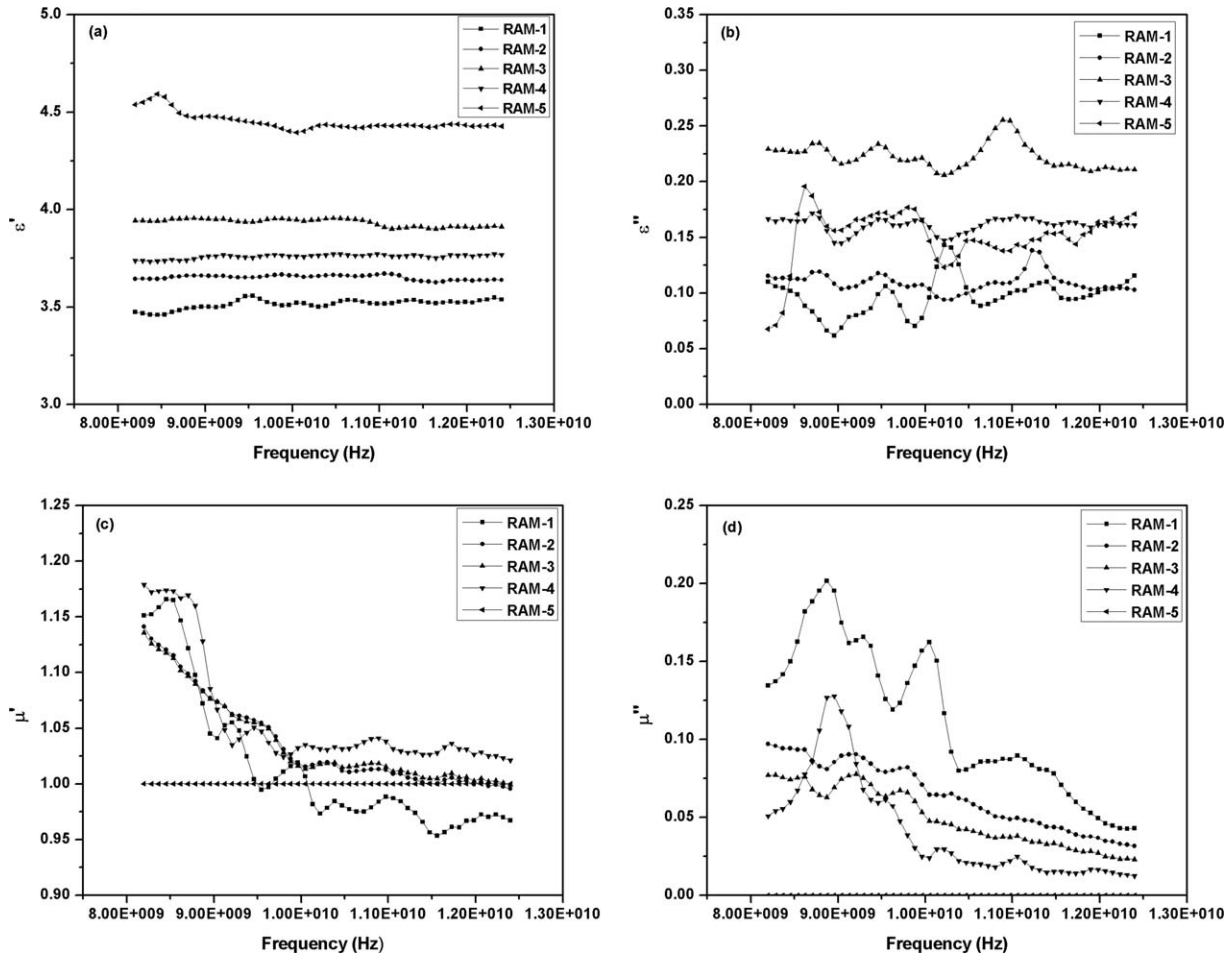

Figure 9. (a) Real (ε') and (b) Imaginary (ε'') parts of complex relative permittivity, (c) Real (μ') and (d) Imaginary (μ'') parts of complex relative permeability of the RAMs.

CONCLUSIONS

Co-doped Ni-Zn ferrite and $BaTiO_3$ nanoparticles were synthesized successfully by coprecipitation and hydrothermal method. The composite materials were fabricated by uniform dispersion of the nanoparticles intothe epoxy resin polymeric matrix. The structure, morphology, thermal stability and electromagnetic properties of the obtained products were characterized by XRD, SEM, TEM, EDS, DLS, TGA, and vector network analyzer. The results show that there have been significant changes in the microwave absorbing properties of the magnetic-dielectric based composites when compared with magnetic composite. Impedance matching effect and thickness matching effect are responsible for achieving the high performance microwave absorbing properties of the composite materials.Out of five RAMs, RAM-3 achieved better microwave absorbing properties with minimum return loss of −42.53 dB at 11.81 GHz when sample thickness was 2 mm. The results indicate that the magnetic loss is less important and the dielectric loss is responsible for microwave absorption and Co-doped Ni-Zn ferrite/$BaTiO_3$ composites have a great potential in the development of lightweight and high efficiency microwave absorbing materials.

ACKNOWLEDGMENTS

The authors especially thank the CSIR, New Delhi, India, for granting the kind financial support for the research work.

REFERENCES

1. Wen, H.; Cao, M.; Sun, G.; Xu, W.; Wang, D.; Zhang, X.; Hu, C. *J. Phys. Chem. B.* **2008**, *112*, 15948.
2. Jana, P. B.; Mallick, A. K.; De, S. K. *IEEE Trans. Electromagn. Compat.* **1992**, *34*, 478.
3. Solomon, M. A.; Kurian, P.; Anantharaman, M. R.; Joy, P. A. *Polym-Plast. Technol.* **2004**, *43*, 1013.
4. Kamchi, N. E.; Belaabed, B.; Wojkiewicz, J. L.; Lamouri, S.; Lasri, T. *J. Appl. Polym. Sci.***2012**.DOI: 10.1002/app.38036.
5. Xiao, H.; Liu, X.; Fu, S. *Compos. Sci. Technol.* **2006**, *66*, 2003.
6. Ling, Q.; Sun, J.; Zhao, Q.; Zhou, Q. *J. Appl. Polym. Sci.* **2009**, *111*, 1911.
7. Shen, X. Z.; Xie, S. M.; Guo, J.; Liu, Z. C. *J. Appl. Polym. Sci.***2009**, *114*, 3434.
8. Aksit, A. C.; Onar, N.; Ebeoglugil, M. F.; Birlik, I.; Celik, E.; Ozdemir, I. *J. Appl. Polym. Sci.***2009**, *113*, 358.
9. Choi, H. D.; Shim, H. W.; Cho, K. Y.; Lee, H. J.; Park, C.S.; Yoon, H. G. *J. Appl. Polym. Sci.***1999**, *72*, 75.
10. Qiu, J.; Lan, L.; Zhang, H.; Gu, M. *J. Alloys. Compd.* **2008**, *453*, 261.
11. Pardavi-Horvath, M. J. *Magn. Magn. Mater.***2000**, *215*, 171.
12. Peng, C. H.; Hwang, C. C.; Wan, J.; Tsai, J. S.; Chen, S. Y. *Mater. Sci. Eng. B.* **2005**, *117*, 27.
13. Singh, P.; Babbar, V. K.; Razdan, A.; Srivastava, S. L.; Goel, T. C. *Mater. Sci. Eng. B.***2000**, *78*, 70.
14. Kim, D. Y.; Chung, Y. C.; Kang, T. W.; Kim, H. C. *IEEE Trans. Magn.* **1996**, *32*, 555.
15. Wu, K. H.; Ting, T. H.; Liu, C. I.; Yang, C. C.; Hsu, J. S. *Compos. Sci. Technol.* **2008**, *68*, 132.
16. Peng, C. H.; Wang, H. W.; Kan, S. W.; Shen, M. Z.; Wei, Y. M.; Chen, S. Y. *J. Magn. Magn. Mater.* **2004**, *284*, 113.
17. Jhao, H.; Ma, R.; Zhang, G.; Li, X. *Integr. Ferroelectr.* **2011**, *127*, 1.
18. Han, R.; Gong, L.; Wang, T.; Qiao, L.; Li, F. *Mater. Chem. Phys.* **2012**, *131*, 555.
19. Das, S.; Mandal, A.; Das C. K. *NanoTrends.* **2012**, *11*, 7.
20. Park, H.K.; Choi, S.H.; Ko, T. *phys. stat. sol. (b).* **2004**, *241*, 1693.
21. Mandal, A.; Das, C. K. *J. Mater. Sci. Res.* **2012**, *1*, 45.
22. Sathishkumar, G.; Venkataraju, C.; Sivakumar, K. *Mater. Sci. Appl.* **2010**, *1*, 19.
23. Snoek, J.L. *Physica (Amsterdam).* **1948**, *14*, 207.
24. Zhao, D. L.; Lv, Q.; Shen, Z. M. *J. Alloys. Compd.***2009**, *480*, 634.
25. Miao, H.; Zhou, Y.; Tan, G.; Dong, M. *J. Electroceram.***2008**, *21*, 553.
26. Tyagi, S.; Baskey, H. B.; Agarwala, R. C.; Agarwalaand, V.; Shami, T. C. *J. Electron.Mater.* **2011**, *40*, 2004.
27. Singh, P.; Babbar, V. K.; Razdan, A.; Srivastava, S. L.; Agrawal, V. K.; Goel, T. C. *J. Mater. Sci.* **2006**, *41*, 7190.
28. Tyagi, S.; Baskey, H. B.; Agarwala, R.; Agarwala, V.; Shami, T. C. T. *Indian I. Metals.* **2011**, *64*, 271.
29. Qiu, J.; Wang, Y.; Gu, M. *J. Mater. Sci.* **2007**, *42*, 166.
30. Pan, X.; Qiu, J.; Gu, M. *J. Mater. Sci.***2007**, *42*, 2086.
31. Abbas, S. M.; Dixit, A. K.; Chatterjee, R.; Goel, T. C. *Mater. Sci. Eng. B.* **2005**, *123*,167.
32. Vander Zaag, P. J. *J. Magn. Magn.Mater.* **1999**, *196*, 315.
33. Wemple, S.H. *Phys. Rev. B.* **1970**, *2*, 2679.
34. Lewis, T. J. *J Phys D: Appl. Phys.***2005**, *38*, 202.
35. Cao, J.; Fu, W.; Yang, H.; Yu, Q.; Zhang, Y.; Liu, S.; Sun, P.; Zhou, X.; Leng, Y.; Wang, S.; Liu, B.; Zou, G. J. *Phys. Chem. B.***2009**, *113*, 4642.